Electronic Supplementary Information (ESI)

Nanorod-like Ni-rich layered cathode with enhanced Li^+ diffusion pathway for high-performance lithium-ion batteries

Fangkun Li[a], Zhengbo Liu[a], Jiadong Shen[a], Xijun Xu[a], Liyan Zeng[a], Binghao Zhang[b], He Zhu[b], Qi Liu[b, *], Jun Liu[a, *], Min Zhu[a]

[a]Guangdong Provincial Key Laboratory of Advanced Energy Storage Materials, School of Materials Science and Engineering, South China University of Technology, Guangzhou 510641, P. R. China, E-mail: msjliu@scut.edu.cn

[b]Department of Physics, City University of Hong Kong, Hong Kong 999077, P. R. China, E-mail: qiliu63@cityu.edu.hk

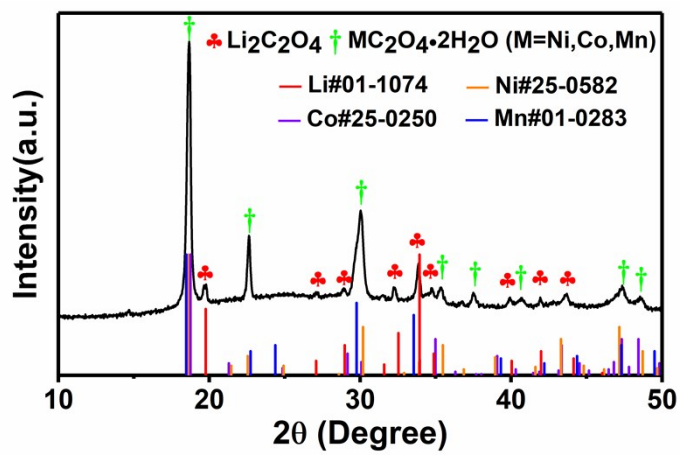

Fig. S1. XRD pattern of $MC_2O_4 \cdot xH_2O$ (M= Li, Ni, Co, Mn) nanorod-like precursors.

This XRD pattern indicates that the precursor $MC_2O_4 \cdot 2H_2O$ (M= Li, Ni, Co and Mn) is composed of $Li_2C_2O_4$ (JCPDS No. 01-1074), $NiC_2O_4 \cdot 2H_2O$ (JCPDS No. 25-0582), $CoC_2O_4 \cdot 2H_2O$ (JCPDS No.25-0250) and $MnC_2O_4 \cdot 2H_2O$ (JCPDS No. 01-0283).

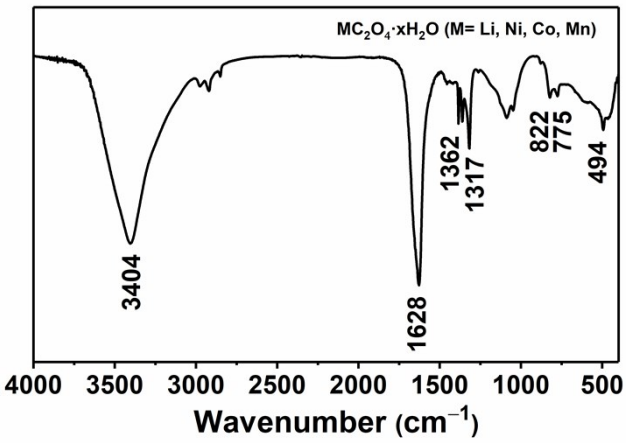

Fig. S2. FT-IR spectrum of $MC_2O_4 \cdot xH_2O$ (M= Li, Ni, Co, Mn) nanorod-like precursor.

According to the FT-IR result, the precursor displays a characteristic spectrum for the presence of hydrated metal oxalates. A broad band at 3404 cm^{-1} originates from H_2O. The strong peak at 1628 cm^{-1} is associated with the C=O stretching vibration and the peaks at 1362 and 1317 cm^{-1} is ascribed to C-O asymmetric and symmetric vibrations. The asymmetric O-C-O band appears at 822 cm^{-1} and M-O bands appear at 775 and 494 cm^{-1}.

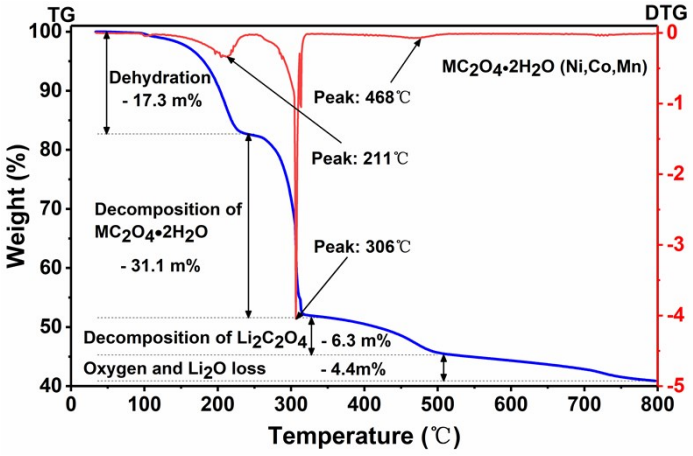

Fig. S3. TG/DTG data of $MC_2O_4 \cdot xH_2O$ (M= Li, Ni, Co, Mn) nanorod-like precursor.

TG/DTG indicates that the first weight loss of about 17.3% in the range of 100–211 ℃ is mainly ascribed to the evaporation of H_2O. The second weight loss of about 31.1% between 240 and 306 ℃ is ascribed to the decomposition of the (Ni, Co, Mn)C_2O_4 and LiC_2O_4. The last weight loss (6.3%) which occurred at the range of 400–468 ℃ is attributed to the decomposition of LiC_2O_4. When improving calcination temperature

and prolonging time, the weight loss of about 4.4% is mainly ascribed to the loss of Li_2O and the partly escape of oxygen from the oxide.

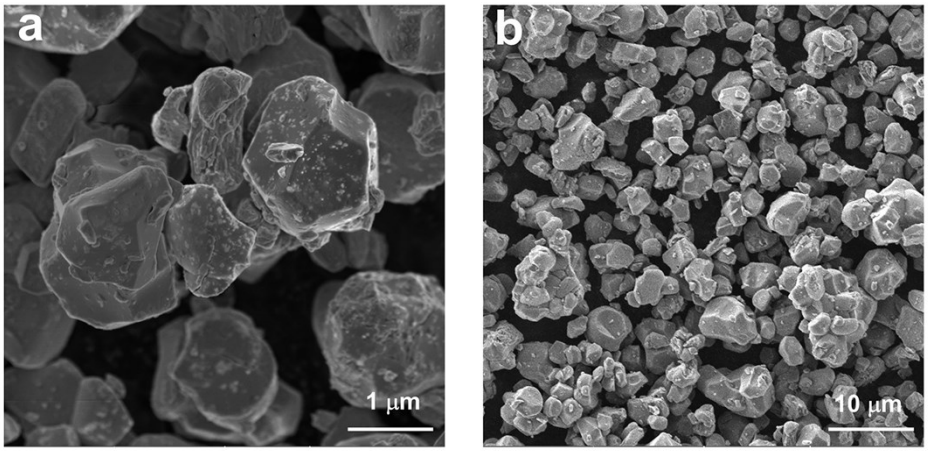

Fig. S4. High- and low-magnification SEM images of C-NCM cathode.

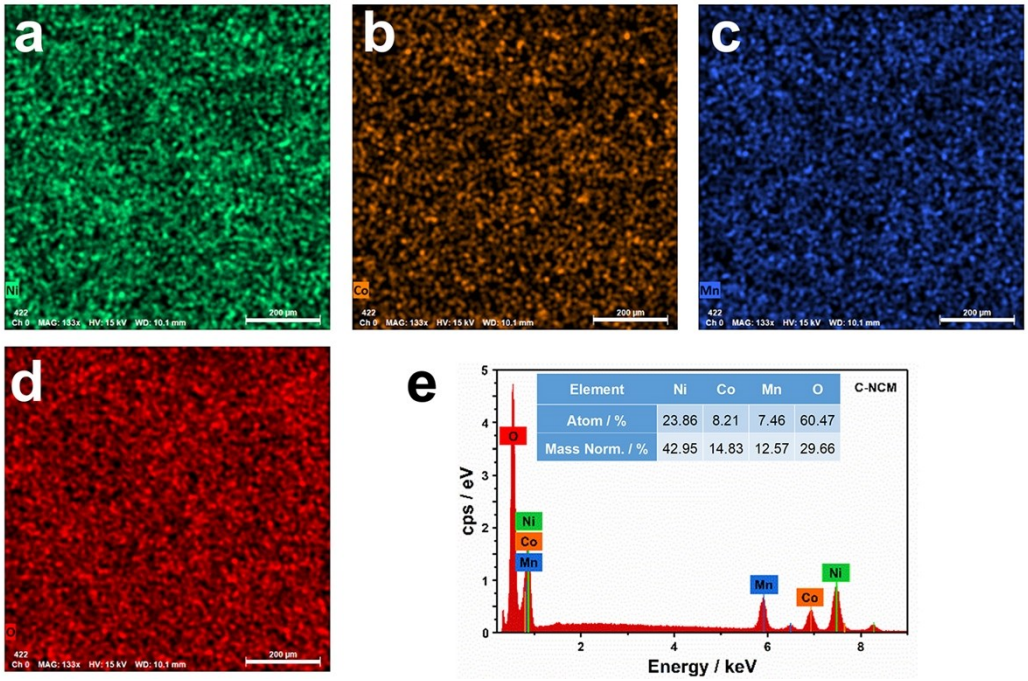

Fig. S5. (a-d) The elemental SEM-EDS mapping of Ni, Co, Mn and O; (e) SEM-EDS spectrum and the corresponding result of elemental compositions of C-NCM cathode.

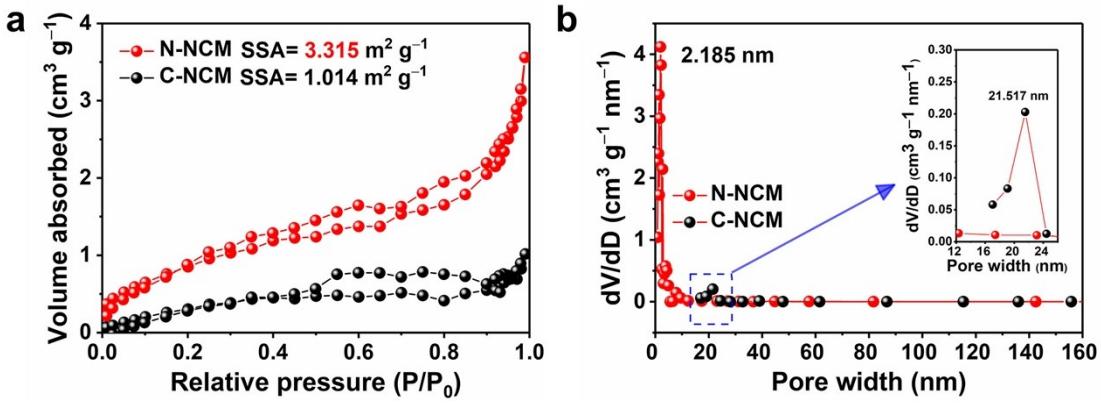

Fig. S6. (a) N_2 adsorption/desorption isotherms and (b) the pore distributions of N-NCM and C-NCM (SSA: specific surface area).

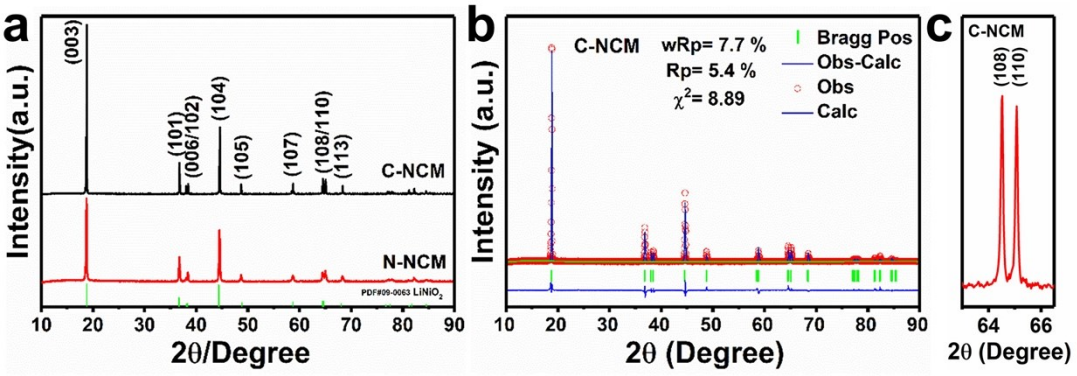

Fig. S7. (a) XRD patterns of N-NCM (red line) and C-NCM (black line); (b) refined and results of C-NCM cathode based on $LiNiO_2$ hexagonal ($R\bar{3}m$) phase; (c) enlarged view of (108) and (110) peaks of C-NCM cathode.

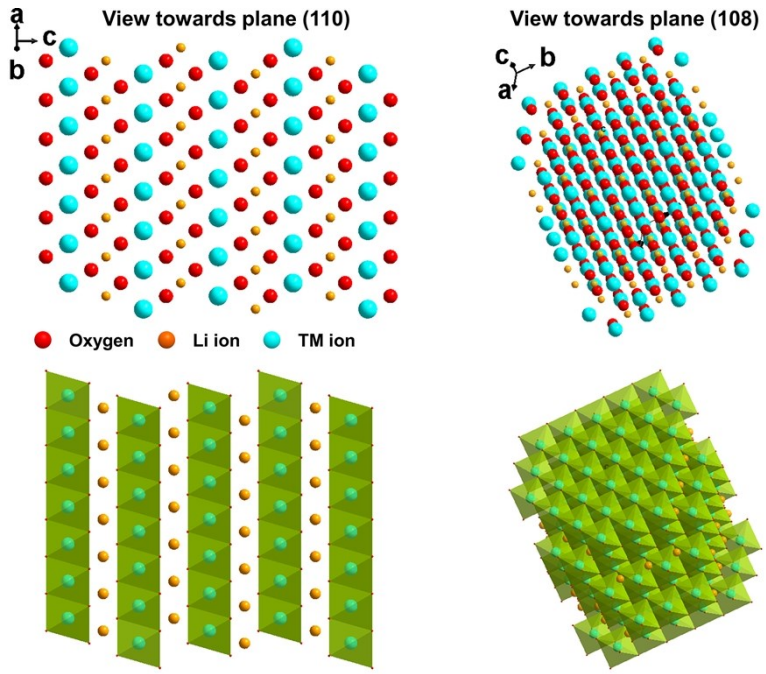

Fig. S8. The crystal structure of hexagonal (R $\bar{3}$m) phase viewed vertically to (110) and (108) planes.

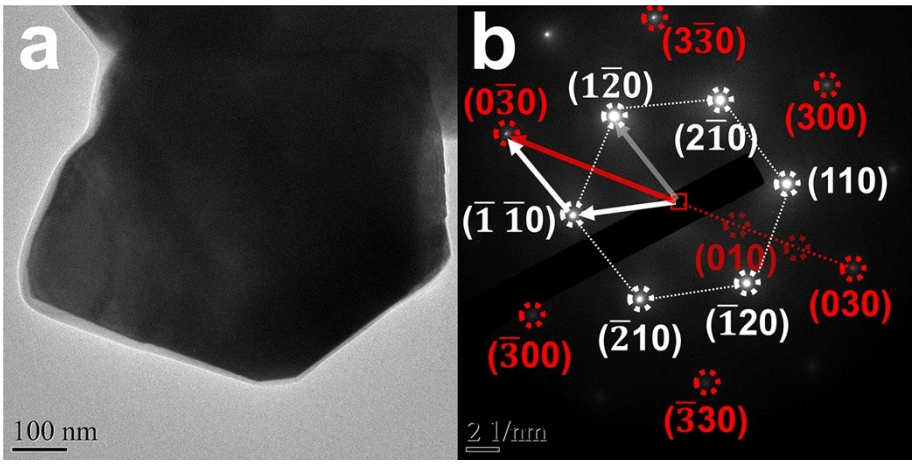

Fig. S9. (a) TEM images and (b) SAED pattern of the N-NCM cathode.

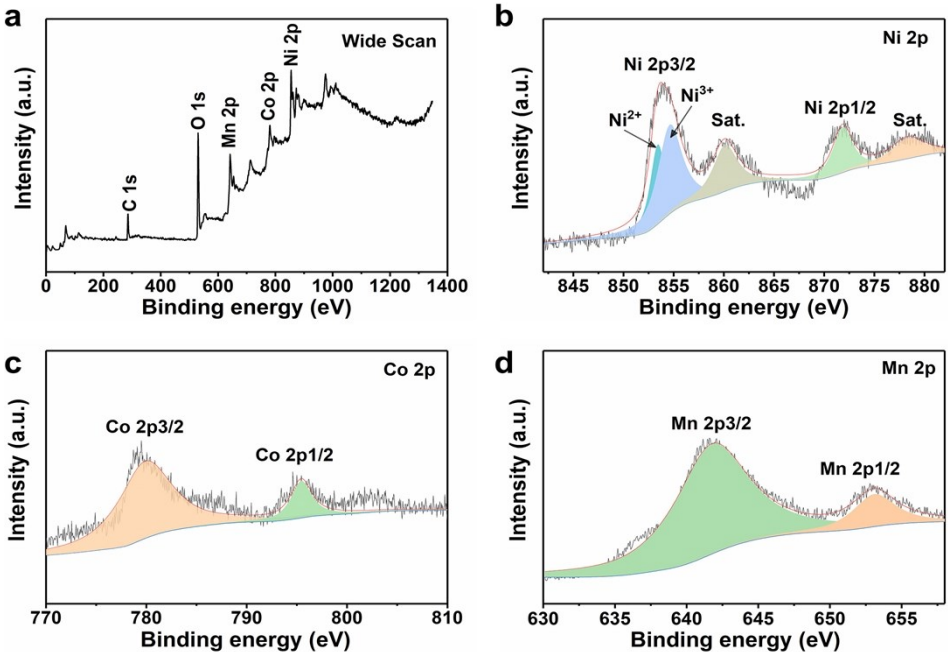

Fig. S10. X-ray photoelectron spectroscopy spectra of N-NCM: (a) wide scan , (b) Ni 2p, (c) Co 2p and (d) Mn 2p.

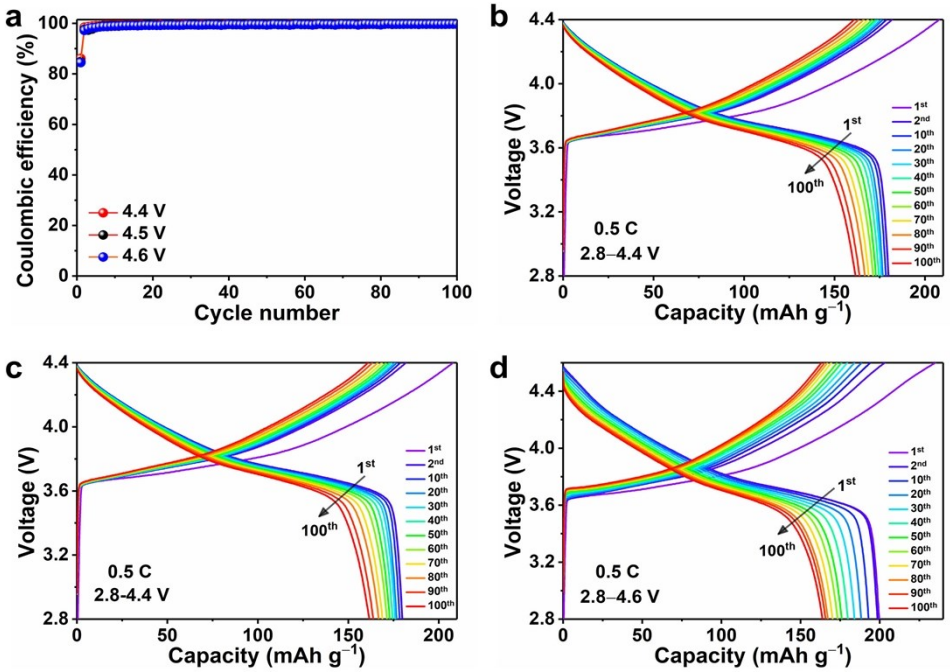

Fig. S11. (a) Coulombic efficiencies of the N-NCM cathode at 0.5 C rate in the various voltage range of 2.8–4.4 ~ 4.6 V for 100 cycles and (c–d) their corresponding charge-

discharge curves at different cycles.

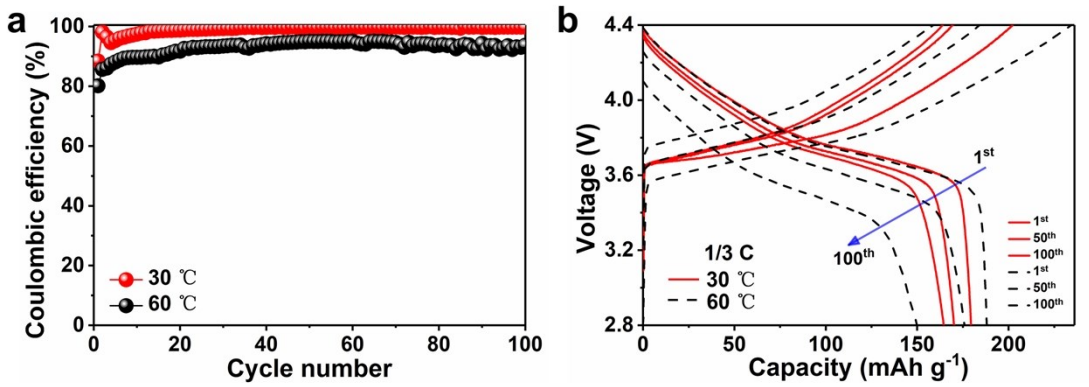

Fig. S12. (a) Coulombic efficiencies of the N-NCM cathode at C/3 rate in the voltage range of 2.8–4.4 V at 30 and 60 ℃ for 100 cycles and (b) their corresponding charge-discharge curves.

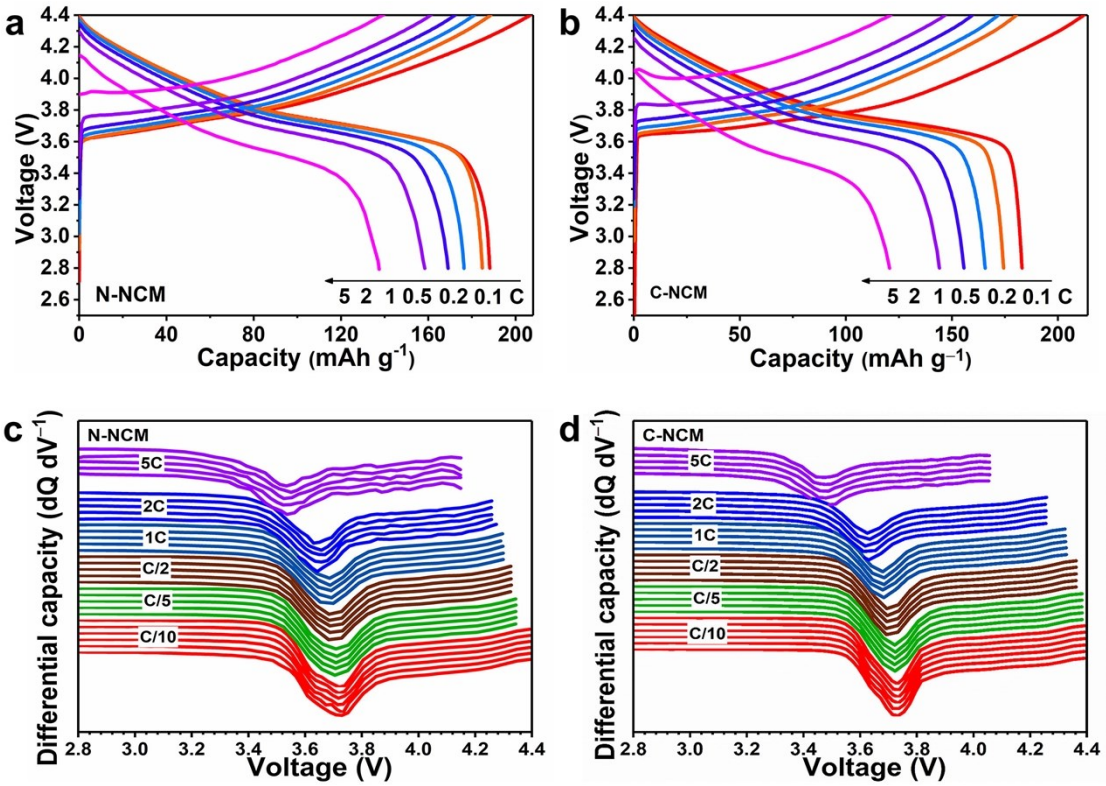

Fig. S13. (a,b) Charge-discharge curves of N-NCM (a) and C-NCM (b) cathodes at various current rates (C/10, C/5, C/2, 1 C, 2 C and 5 C) in the voltage range of 2.8–4.4

V; (c,d) Differential capacity curves of N-NCM (c) and C-NCM (d) cathodes obtained from the discharge at different current rates.

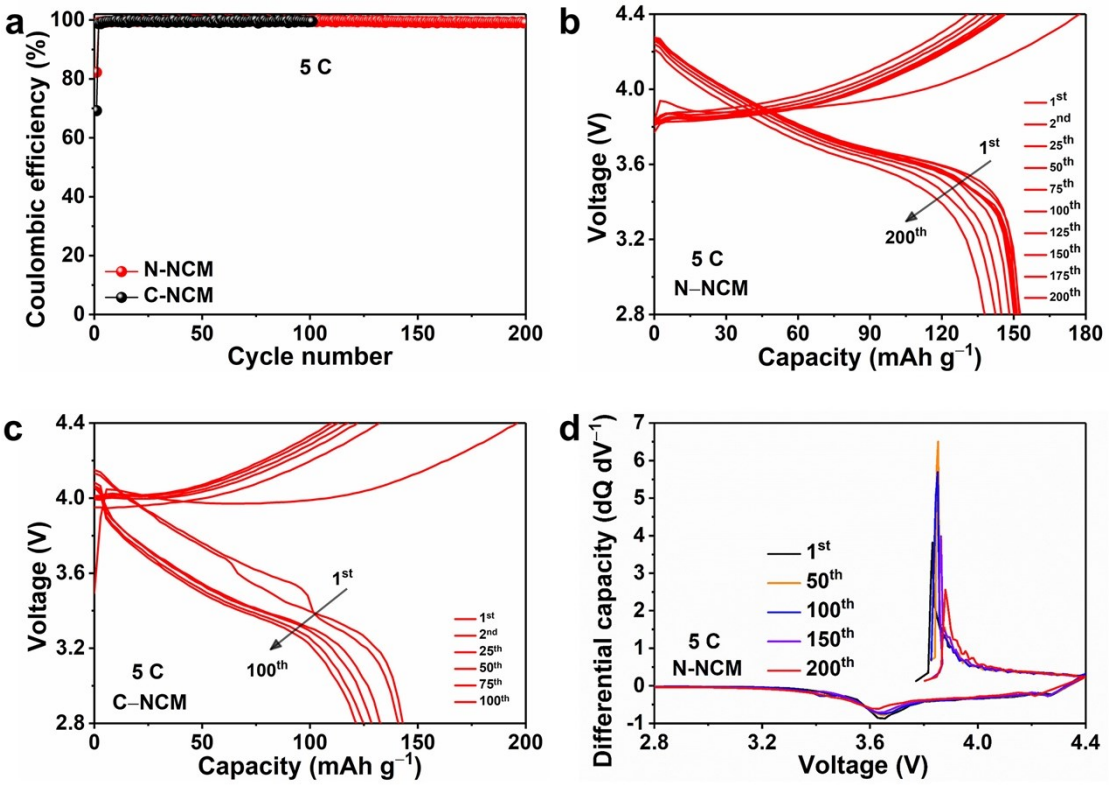

Fig. S14. (a) the Coulombic efficiencies and (b, c) charge-discharge curves of the N-NCM and C-NCM cathode at 5 C rate for long-term cycles, and (d) differential capacity curves of N-NCM electrode.

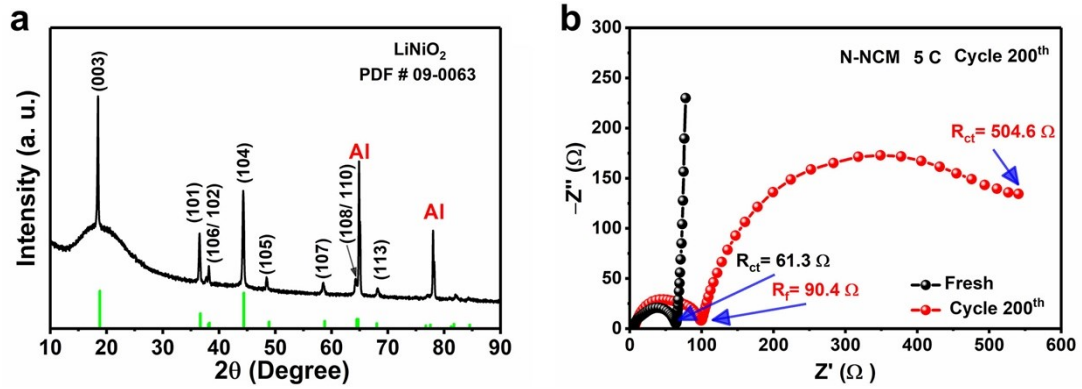

Fig. S15. (a) XRD patterns and (b) Nyquist plots of N-NCM cathode after 200th cycles over 2.8–4.4 V at 5 C rate.

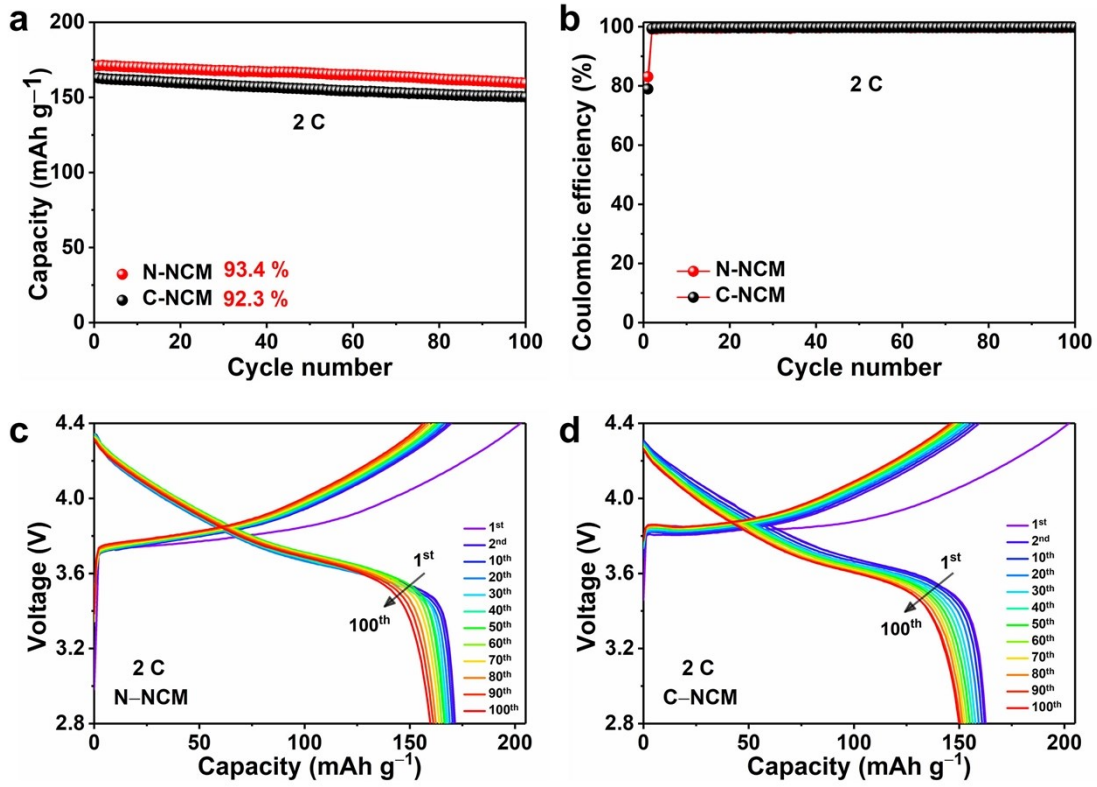

Fig. S16. (a) Cycling performance and (b) Coulombic efficiencies of the N-NCM and C-NCM cathode at 2 C rate for 100 cycles and (c,d) their corresponding charge and discharge curves.

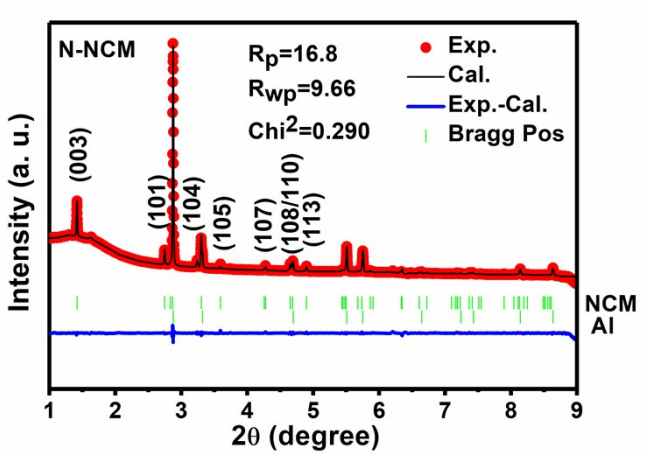

Fig. S17. Refined and results of N-NCM cathode based on $LiNiO_2$ hexagonal ($R\bar{3}m$) phase and Al phase.

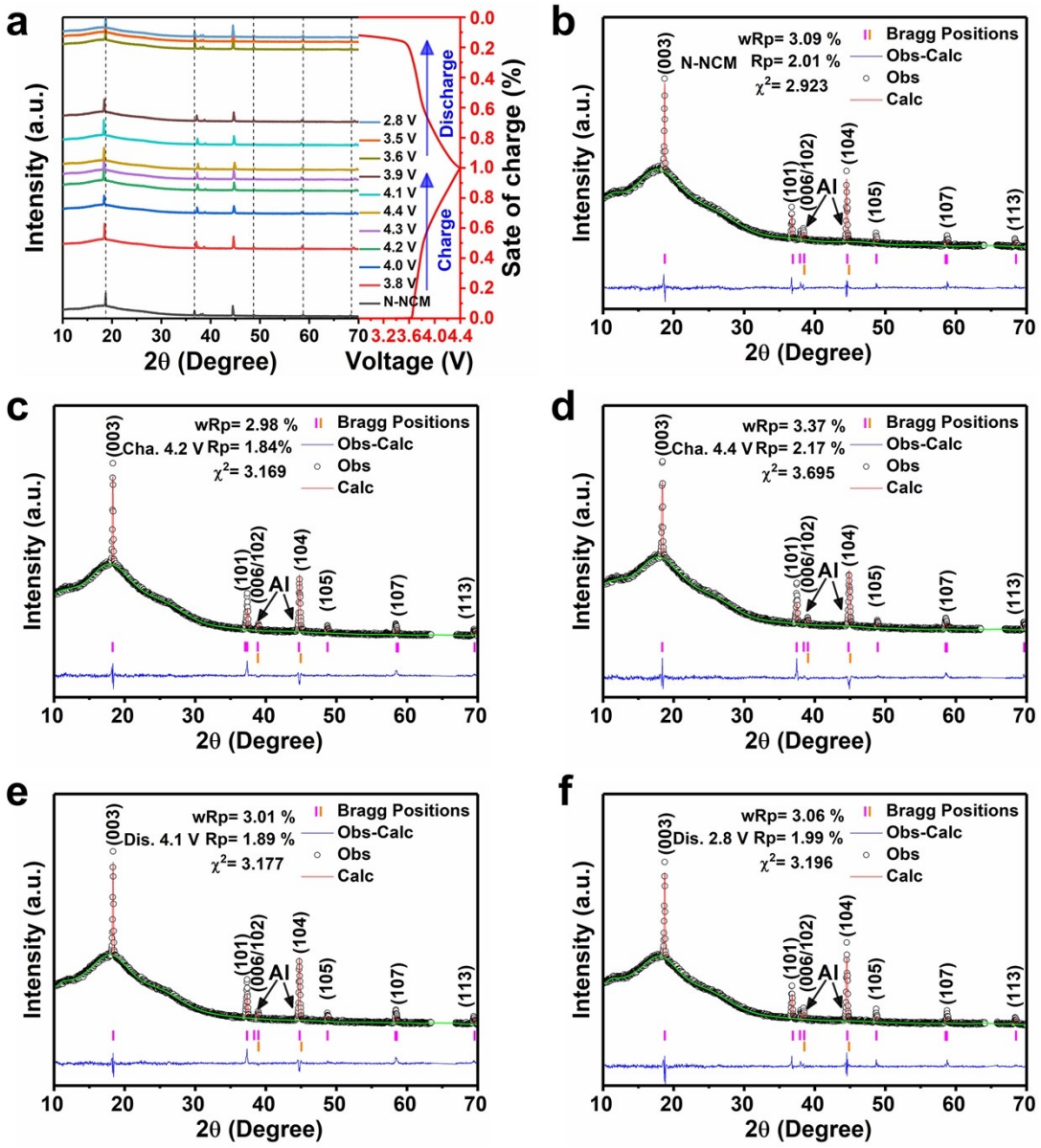

Fig. S18. (a) *ex-situ* XRD patterns during the first charge/discharge process of N-NCM electrode under a current of C/10 at different cut-off voltage. (b-f) Refined and results of N-NCM cathode based on $LiNiO_2$ hexagonal ($R\bar{3}m$) phase and Al phase (Cha.: Charge, Dis.: Discharge).

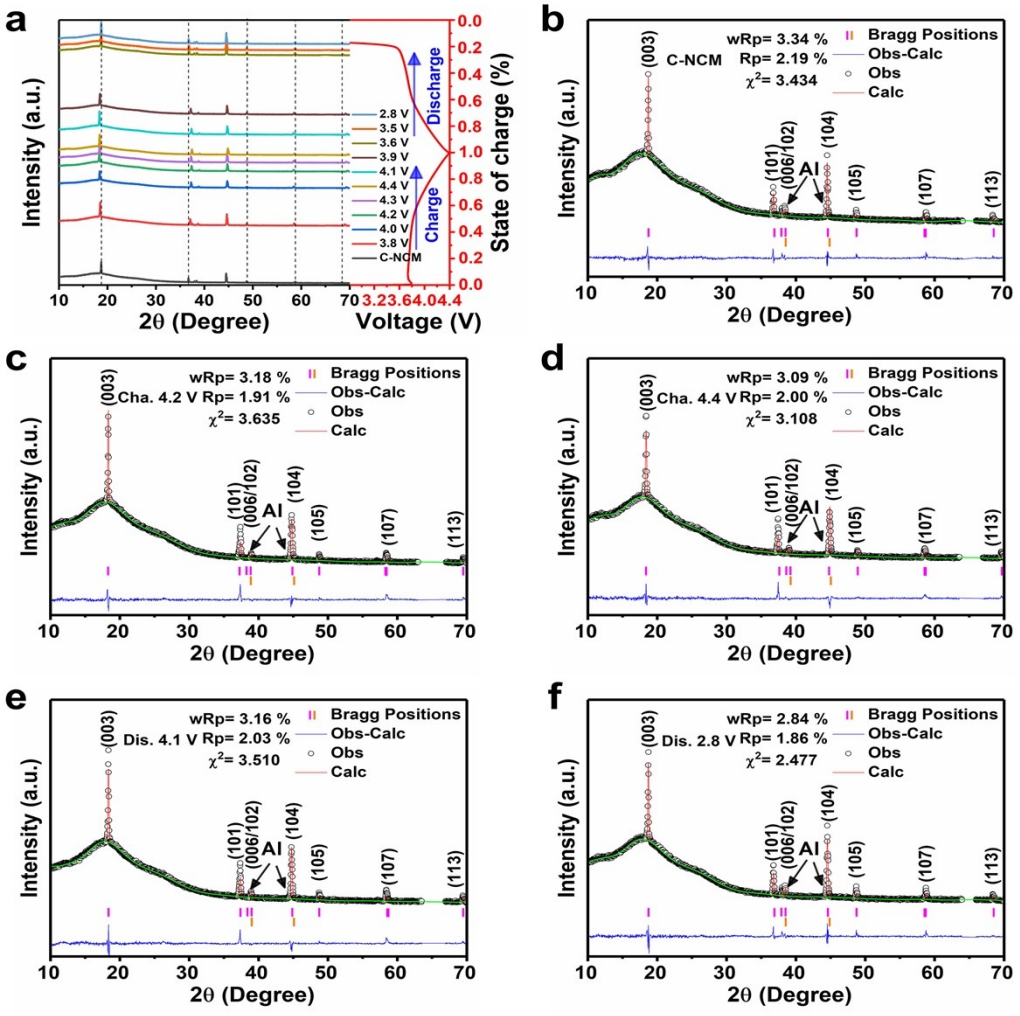

Fig. S19. (a) *ex-situ* XRD patterns during the first charge/discharge process of C-NCM electrode under a current of C/10 at different cut-off voltage. (b-f) Refined and results of C-NCM cathode based on $LiNiO_2$ hexagonal ($R\bar{3}m$) phase and Al phase (Cha.: Charge, Dis.: Discharge).

All *ex-situ* XRD patterns were refined and analyzed by using GSAS software. The lattice parameters extracted from each *ex-situ* XRD pattern are listed in the following Table S7 and Table S8, in which a=b due to the nature of hexagonal phase. As in result, the nanorod-like N-NCM cathode exhibits a smaller volume change (1.93%) than the

C-NCM ones (2.11%).

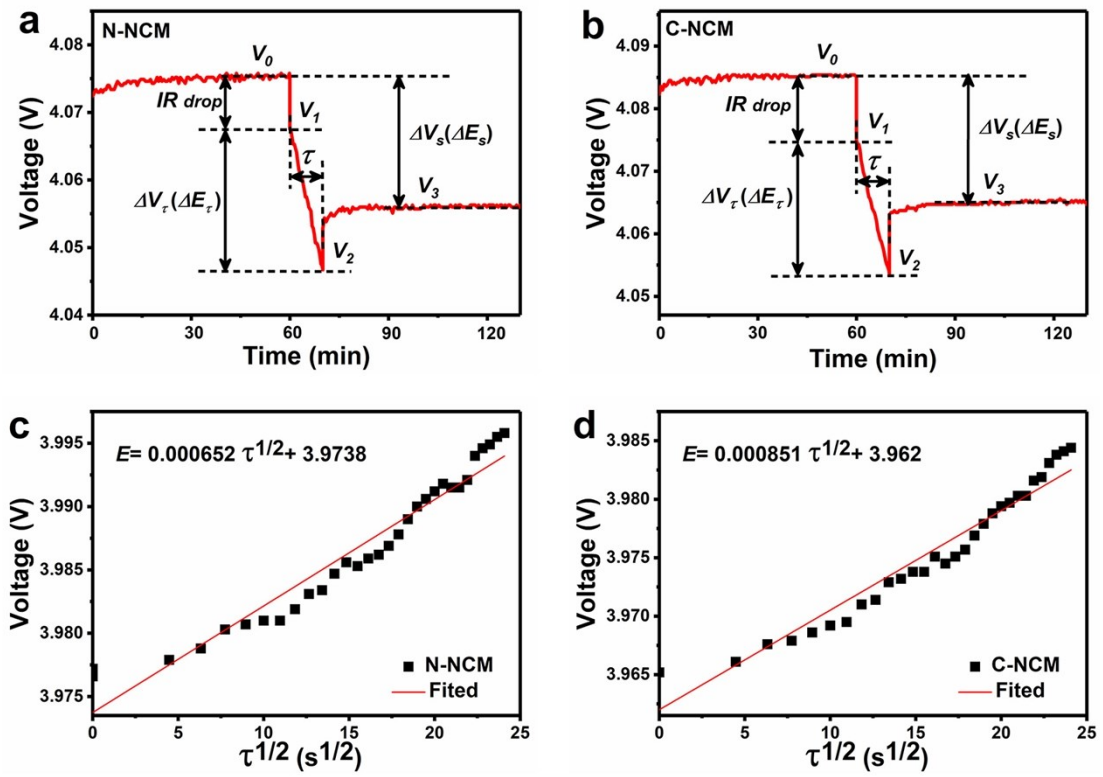

Fig. S20. (a,b) Applied current plus *vs.* cell voltage for a single titration step of GITT curves; (c,d) linear fit of the cell voltage as a function of the square root of time ($\tau^{1/2}$) with different pulse currents.

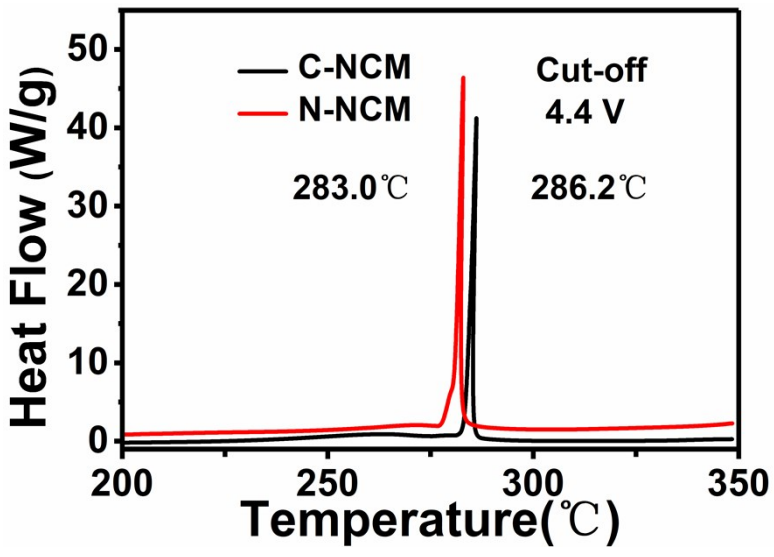

Fig. S21. DSC profiles of N-NCM (red line) and C-NCM (black line) after charging at 4.4 V.

Table S1. Crystallographic data for N-NCM.

Radiation	Powder X-ray (Cu Kα) λ=1.54 Å
Crystal system	Hexagonal
Space group	$R\bar{3}m$ (No. 166)
Lattice parameters (Å)	a=b=2.86550(4), c=14.19627(24), α=β= 90°, γ=120°
Cell volume	100.9498(25) $Å^3$
c/*a*	4.954
$I_{(003)}/I_{(104)}$	1.49
Rwp	4.8%
Rp	2.7%
χ^2	2.87

Table S2. Atomic site information for N-NCM

Atom	Wyck.	a	b	c	Occ.	Ui/Ue*100
Li1	3a	0	0	0	0.946	3.39

Ni2	3a	0	0	0	0.054	3.39
Li2	3b	0	0	0.5	0.010	2.00
Ni1	3b	0	0	0.5	0.590	2.00
Co1	3b	0	0	0.5	0.200	2.00
Mn1	3b	0	0	0.5	0.200	2.00
O2	6c	0	0	0.25861(12)	1.000	1.38(7)

Table S3. Crystallographic data for C-NCM.

Radiation	Powder X-ray (Cu Kα) λ=1.54 Å
Crystal system	Hexagonal
Space group	$R\bar{3}m$ (No. 166)
Lattice parameters (Å)	a=b=2.86749(3), c=14.20843(14), α=β= 90°, γ=120°
Cell volume	101.1768(19) $Å^3$
c/*a*	2.955
$I_{(003)}/I_{(104)}$	2.37
Rwp	7.7%
Rp	5.4%

χ^2	8.89

Table S4. Atomic site information for C-NCM

Atom	Wyck.	a	b	c	Occ.	Ui/Ue*100
Li1	3a	0	0	0	0.9974	7.26
Ni2	3a	0	0	0	0.0026	7.26
Li2	3b	0	0	0.5	0.0100	3.50
Ni1	3b	0	0	0.5	0.5900	3.50
Co1	3b	0	0	0.5	0.2000	3.50
Mn1	3b	0	0	0.5	0.2000	3.50
O2	6c	0	0	0.267618	1.0000	3.09

Table S5. Electrochemical performance comparison (capacity, rate capability and cycling stability) of N-NCM cathode with reported $LiN_{i0.6}Co_{0.2}Mn_{0.2}O_2$-based materials.

Reference	Cut-off Volatge (V)	1 C (mA g^{-1})	Capacity (mAh g^{-1})	Rate Capacity (mAh g^{-1})	Cycling Retention
$LiAlO_2$-coated	2.7–4.5	250	206.8 (0.2 C)	142 (3 C)	72.1% after 350

NCM[1]					cycles at 0.2 C
$BaTiO_3$ modified NCM[2]	3.0–4.5	--	189 (0.2 C)	140 (10 C)	86.6% after 200 cycles at 5 C
TiO_2-coated NCM[3]	3.0–4.5	140	177.3 (1 C)	144.5 (5 C)	88.7% after 50 cycles at 1 C
dual-conductive polymer coated NCM[4]	2.8–4.3	180	184.3 (0.1 C)	166.0 (5 C)	93.9% after 100 cycles at 0.5 C
SiO_2-coated NCM[5]	3.0–4.3	--	175.7 (0.1 C)	153.2 (2 C)	95% after 50 cycles at 0.5 C
TiO_2-coated NCM[6]	2.5–4.3	--	187.7 (0.1 C)	130.2 (5 C)	85.9% after 100 cycles at 1 C
Li_xTiO_2@Si-coated NCM[7]	2.75–4.3	180	178.9 (0.5 C)	141 (5 C)	--
gradient phosphate polyanion doped NCM[8]	2.7–4.5	--	178.5 (0.5 C)	131 (5 C)	88.8% after 100 cycles at 0.5 C
Ta-doped NCM[9]	3.0–4.5	180	188.2 (0.2 C)	--	83.6% after 100

					cycles at 1 C
ZnO modified NCM[10]	2.7–4.5	--	194.8 (0.2 C)	150 (3 C)	68% after 300 cycles at 0.2 C
Mg-doped NCM[11]	2.7–4.3	180	184 (0.05 C)	138 (2 C)	--
Cu modified NCM[12]	3.0–4.3	--	186 (0.05 C)	153.3 (2 C)	94.9% after 90 cycles at 0.33 C
Microrod NCM[13]	2.7–4.3	180	162 (0.1 C)	105 (5 C)	87.1% after 100 cycles at 0.1 C
This word	2.8-4.4	180	188.2 (0.1 C)	158.8 (2 C) 128.4 (5 C)	95.4% after 100 cycles at C/3 93.4% after 100 cycles at 2 C 90.6% after 200 cycles at 5 C

Table S6. The lattice parameters extracted from each XRD patterns

	H1			H2		
	a-axis/ Å	b-axis/ Å	c-axis/ Å	a-axis/ Å	b-axis/ Å	c-axis/ Å
1	2.86732(7)	2.86732(7)	14.2108(6)			
2	2.86752(6)	2.86752(6)	14.2105(5)			
3	2.86635(8)	2.86635(8)	14.2085(6)			
4	2.86528(5)	2.86528(5)	14.2089(6)			
5	2.86583(7)	2.86583(7)	14.2149(5)			
6	2.86520(7)	2.86520(7)	14.2150(5)			
7	2.86477(5)	2.86477(5)	14.2159(6)			
8	2.86483(7)	2.86483(7)	14.2174(6)			
9	2.86445(7)	2.86445(7)	14.2201(6)			
10	2.86401(7)	2.86401(7)	14.2269(6)			
11	2.86416(7)	2.86416(7)	14.2266(6)			
12	2.86297(8)	2.86297(8)	14.2281(6)			
13	2.86313(7)	2.86313(7)	14.2236(6)			
14	2.86300(7)	2.86300(7)	14.2263(6)			

15	2.86282(7)	2.86282(7)	14.2279(6)			
16	2.86191(8)	2.86191(8)	14.2330(9)			
17	2.86196(8)	2.86196(8)	14.2322(6)			
18	2.86187(8)	2.86187(8)	14.2366(6)			
19	2.86141(8)	2.86141(8)	14.2379(6)			
20	2.86104(7)	2.86104(7)	14.2380(6)			
21	2.86079(8)	2.86079(8)	14.2380(6)			
22	2.86025(9)	2.86025(9)	14.2410(6)			
23	2.86008(8)	2.86008(8)	14.2447(6)			
24	2.85905(7)	2.85905(7)	14.2461(6)			
25	2.85902(7)	2.85902(7)	14.2501(6)			
26	2.85690(9)	2.85690(9)	14.2584(9)			
27	2.85885(8)	2.85885(8)	14.2418(9)			
28	2.85769(9)	2.85769(9)	14.2530(8)			
29	2.85726(8)	2.85726(8)	14.2558(9)			
30	2.85749(8)	2.85749(8)	14.2539(9)			
31	2.85676(7)	2.85676(7)	14.2500(9)			

32	2.85566(8)	2.85566(8)	14.2619(9)			
33	2.85295(9)	2.85295(9)	14.2868(9)			
34	2.8553(1)	2.8553(1)	14.284(2)	2.8464(1)	2.8464(1)	14.299(1)
35	2.8541(1)	2.8541(1)	14.287(1)	2.8444(1)	2.8444(1)	14.313(2)
36	2.8494(3)	2.8494(3)	14.317(2)	2.8395(4)	2.8395(4)	14.332(3)
37	2.8551(2)	2.8551(2)	14.252(2)	2.8360(2)	2.8360(2)	14.364(2)
38	2.8422(3)	2.8422(3)	14.333(3)	2.8323(3)	2.8323(3)	14.397(3)
39	2.8454(4)	2.8454(4)	14.321(2)	2.82791(9)	2.82791(9)	14.397(1)
40	2.8295(4)	2.8295(4)	14.403(2)	2.82804(9)	2.82804(9)	14.4171(4)
41				2.8267(1)	2.8267(1)	14.417(1)
42				2.82403(9)	2.82403(9)	14.4087(8)
43				2.82391(9)	2.82391(9)	14.4287(9)
44				2.8232(1)	2.8232(1)	14.446(2)
45				2.8214(1)	2.8214(1)	14.440(1)
46				2.82075(9)	2.82075(9)	14.4473(7)
47				2.8202(1)	2.8202(1)	14.445(2)
48				2.81936(9)	2.81936(9)	14.4513(8)

49				2.8186(2)	2.8186(2)	14.451(1)
50				2.8180(2)	2.8180(2)	14.449(1)
51				2.81750(9)	2.81750(9)	14.4419(9)
52				2.81738(9)	2.81738(9)	14.4578(9)
53				2.81715(6)	2.81715(6)	14.4524(5)
54				2.8162(2)	2.8162(2)	14.445(2)
55				2.8155(2)	2.8155(2)	14.428(2)
56				2.8156(2)	2.8156(2)	14.430(2)
57				2.8160(2)	2.8160(2)	14.436(2)
58				2.81654(9)	2.81654(9)	14.4430(9)
59				2.8160(2)	2.8160(2)	14.437(3)
60				2.8161(2)	2.8161(2)	14.435(1)
61				2.81676(9)	2.81676(9)	14.4527(9)
62				2.8170(2)	2.8170(2)	14.450(1)
63				2.8176(2)	2.8176(2)	14.453(3)
64				2.8169(2)	2.8169(2)	14.442(2)
65				2.81819(8)	2.81819(8)	14.456(1)

66				2.8192(2)	2.8192(2)	14.453(2)
67				2.8193(2)	2.8193(2)	14.452(1)
68				2.8197(2)	2.8197(2)	14.448(1)
69				2.8206(2)	2.8206(2)	14.4434(1)
70				2.8211(2)	2.8211(2)	14.443(1)
71				2.8220(2)	2.8220(2)	14.439(1)
72				2.8220(2)	2.8220(2)	14.431(1)
73				2.8227(2)	2.8227(2)	14.428(1)
74				2.8235(2)	2.8235(2)	14.422(1)
75				2.82865(9)	2.82865(9)	14.4173(9)
76				2.8278(2)	2.8278(2)	14.390(1)
77				2.8279(2)	2.8279(2)	14.3823(9)
78				2.8305(2)	2.8305(2)	14.407(1)
79				2.8295(2)	2.8295(2)	14.374(1)
80				2.8319(1)	2.8319(1)	14.400(1)
81				2.8324(1)	2.8324(1)	14.3888(9)
82				2.83353(9)	2.83353(9)	14.390(2)

83				2.83433(9)	2.83433(9)	14.388(1)
84				2.8354(1)	2.8354(1)	14.392(1)
85				2.83578(9)	2.83578(9)	14.388(1)
86				2.8363(1)	2.8363(1)	14.383(1)
87				2.83814(9)	2.83814(9)	14.3752(9)
88				2.8384(1)	2.8384(1)	14.375(1)
89				2.8372(1)	2.8372(1)	14.367(1)
90				2.8414(1)	2.8414(1)	14.363(1)
91				2.8418(1)	2.8418(1)	14.359(1)
92				2.8422(1)	2.8422(1)	14.361(1)
93				2.8434(1)	2.8434(1)	14.348(1)
94				2.8447(1)	2.8447(1)	14.344(1)
95				2.8454(1)	2.8454(1)	14.337(1)
96				2.8463(1)	2.8463(1)	14.329(1)
97				2.8476(1)	2.8476(1)	14.326(1)
98				2.8482(1)	2.8482(1)	14.319(1)
99				2.8496(1)	2.8496(1)	14.312(1)

100				2.85087(7)	2.85087(7)	14.3055(8)
101				2.85231(7)	2.85231(7)	14.2983(8)
102				2.85514(7)	2.85514(7)	14.2790(8)
103				2.85649(7)	2.85649(7)	14.2716(8)
104				2.85699(7)	2.85699(7)	14.2646(8)
105				2.85652(7)	2.85652(7)	14.2683(8)
106				2.85637(7)	2.85637(7)	14.2696(8)

Table S7. The lattice parameters extracted from each *ex-situ* XRD patterns of N-NCM at different cut-off voltage.

	a (Å)	**c (Å)**	**V (Å^3)**	**χ^2**	**wRp (%)**	**Rp (%)**
Fresh	2.86516(9)	14.2016(8)	100.964(7)	2.923	3.09	2.01
Cha. 3.8 V	2.83779(8)	14.3798(6)	100.287(6)	3.720	3.31	2.08
Cha. 4.0 V	2.82369(14)	14.4586(11)	99.837(10)	3.597	3.28	2.05
Cha. 4.2 V	2.81526(10)	14.5177(7)	99.648(7)	3.169	2.98	1.84
Cha. 4.3 V	2.82445(12)	14.4676(9)	99.953(9)	3.836	3.25	2.06
Cha 4.4 V	2.81139(12)	14.4650(10)	99.014(9)	3.695	3.37	2.17

Dis. 4.1 V	2.81821(9)	14.4994(7)	99.730(7)	3.177	3.01	1.89
Dis. 3.9 V	2.82976(10)	14.4267(8)	100.045(8)	3.232	3.07	1.92
Dis. 3.6 V	2.86029(9)	14.2352(9)	100.841(6)	4.214	3.44	2.17
Dis. 3.5 V	2.85998(12)	14.2352(9)	100.837(9)	3.879	3.35	2.09
Dis. 2.8 V	2.86331(10)	14.2184(7)	100.952(7)	3.196	3.06	1.99

Note: Cha.: Charge, Dis.: Discharge.

Table S8. The lattice parameters extracted from each *ex-situ* XRD patterns of C-NCM at different cut-off voltage.

	a (Å)	**c (Å)**	**V (Å^3)**	**χ^2**	**wRp (%)**	**Rp (%)**
Fresh	2.86518(7)	14.2187(6)	101.086(6)	3.434	3.34	2.19
Cha. 3.8 V	2.83783(3)	14.3798(6)	100.290(6)	3.499	3.21	2.00
Cha. 4.0 V	2.82381(14)	14.4594(12)	99.851(11)	3.685	3.31	2.00
Cha. 4.2 V	2.81558(12)	14.5278（6）	99.739（8）	3.635	3.18	1.91
Cha. 4.3 V	2.82446(11)	14.4676(9)	99.953(8)	3.536	3.12	1.93
Cha 4.4 V	2.81083(10)	14.4614(8)	98.949(7)	3.108	3.09	2.00
Dis. 4.1 V	2.81819(11)	14.4998(8)	99.731(8)	3.510	3.16	2.03

Dis. 3.9 V	2.82963(10)	14.4270(8)	100.038(8)	3.151	3.03	1.91
Dis. 3.6 V	2.86030(9)	14.2331(7)	100.845(7)	4.436	3.54	2.27
Dis. 3.5 V	2.85699(12)	14.2345(9)	100.832(9)	3.665	3.24	2.03
Dis. 2.8 V	2.86472(8)	14.2179(5)	101.049(5)	2.477	2.84	1.86

Note: Cha.: Charge, Dis.: Discharge.

Reference in ESI.

1. W. Liu, X. Li, D. Xiong, Y. Hao, J. Li, H. Kou, B. Yan, D. Li, S. Lu, A. Koo, K. Adair and X. Sun, *Nano Energy*, 2018, **44**, 111–120.

2. W. Wang, L. Wu, Z. Li, S. Ma, H. Dou and X. Zhang, *ChemElectroChem*, 2020, **7**, 3646–3652.

3. Y. Chen, Y. Zhang, B. Chen, Z. Wang and C. Lu, *J. Power Sources*, 2014, **256**, 20–27.

4. S. H. Ju, I. S. Kang, Y. S. Lee, W. K. Shin, S. Kim, K. Shin and D. W. Kim, *ACS Appl. Mater. Interfaces*, 2014, **6**, 2546–2552.

5. W. Cho, S.-M. Kim, J. H. Song, T. Yim, S.-G. Woo, K.-W. Lee, J.-S. Kim and Y.-J. Kim, *J. Power Sources*, 2015, **282**, 45–50.

6. C. Qin, J. Cao, J. Chen, G. Dai, T. Wu, Y. Chen, Y. Tang, A. Li and Y. Chen, *Dalton Trans*, 2016, **45**, 9669–9675.

7. S. Guo, B. Yuan, H. Zhao, D. Hua, Y. Shen, C. Sun, T. Chen, W. Sun, J. Wu, B. Zheng, W. Zhang, S. Li and F. Huo, *Nano Energy*, 2019, **58**, 673–679.

8. Q. Ran, H. Zhao, Q. Wang, X. Shu, Y. Hu, S. Hao, M. Wang, J. Liu, M. Zhang, H. Li, N. Liu and X. Liu, *Electrochim. Acta*, 2019, **299**, 971–978.

9. B. Chu, S. Liu, L. You, D. Liu, T. Huang, Y. Li and A. Yu, *ACS Sustainable Chem. Eng.*, 2020, **8**, 3082–3090.

10. Y. Li, X. Li, J. Hu, W. Liu, H. Maleki Kheimeh Sari, D. Li, Q. Sun, L. Kou, Z. Tian, L. Shao, C. Zhang, J. Zhang and X. Sun, *Energy Environ. Mater.*, 2020, DOI: 10.1002/eem2.12080.

11. A. L. Lipson, J. L. Durham, M. LeResche, I. Abu-Baker, M. J. Murphy, T. T. Fister, L. Wang, F. Zhou, L. Liu, K. Kim and D. Johnson, *ACS Appl. Mater. Interfaces*, 2020, **12**, 18512–18518.

12. R. Zhang, Z. Meng, X. Ma, M. Chen, B. Chen, Y. Zheng, Z. Yao, P. Vanaphuti, S. Bong, Z. Yang and Y. Wang, *Nano Energy*, 2020, **78**,105214.

13. Y.-Y. He, C.-Q. Zhu, K.-H. Hu, K. Zhou, Y. Qing, X.-L. Yan, Y. Liu, E.-Q. Yang, C.-M. Yang and N.-C. Chen, *Ionics*, 2019, **25**, 5277–5285.